energies

MDPI

Review

Novel Spinel Nanomaterials for Photocatalytic Hydrogen Evolution Reactions: An Overview

Swapnali Walake, Yogesh Jadhav * and Atul Kulkarni *

Symbiosis Centre for Nanoscience and Nanotechnology, Symbiosis International (Deemed University) Lavale, Pune 412115, India; swapnali.rabade@scnn.edu.in

* Correspondence: yogesh.jadhav@scnn.edu.in (Y.J.); atul.kulkarni@scnn.edu.in (A.K.)

Abstract: The energy demand generated by fossil fuels is increasing day by day, and it has drastically increased after the COVID-19 pandemic as industries and household utilities rejuvenate. Renewable sources are thus becoming more essential as easily available, alternative methods of low-cost energy generation. Among these renewables, solar energy, i.e., solar power, is a promising energy source and can be used for solar-based H_2 evolution because H_2 technology is a leading source of eco-friendly electricity generation, and most of the worldwide efforts to develop this method involve heterogeneous catalysis for H_2 evolution via water splitting and its storage, i.e., using a fuel cell. In the current scenario, there is a need to develop a stable, recyclable, and reusable heterogeneous catalyst system, which is a great challenge. In the current study, we have focused on novel ferrite magnetic nanomaterials for recyclable and reusable robust photocatalysis. Moreover, discussions of the factors contributing to the photocatalytic hydrogen evolution, low-cost synthesis techniques, and prospects for making them ideal photocatalysts are uncommon in the literature. The study will impart possible approaches for the design and development of novel ferrite nanomaterials and their nanocomposites for H_2 generation in the forthcoming years.

Keywords: renewable energy; H_2 evolution; solar power; recyclable; stable; synthesis approaches; photocatalysis; spinel ferrites; nanomaterials

check for updates

Citation: Walake, S.; Jadhav, Y.; Kulkarni, A. Novel Spinel Nanomaterials for Photocatalytic Hydrogen Evolution Reactions: An Overview. *Energies* **2023**, *16*, 4707. https://doi.org/10.3390/en16124707

Academic Editor: Frede Blaabjerg

Received: 18 May 2023
Revised: 5 June 2023
Accepted: 8 June 2023
Published: 14 June 2023

1. Introduction

Traditionally, non-renewable energy sources termed fossil fuels, including coal, oil, nuclear energy, and natural gas, are used in huge amounts for power generation in industries and domestic settings due to the increased demand for petroleum and automobiles. Attention to renewable energy sources, known as clean energy sources, including wind, solar, water, geothermal, and biomass, is increasing, mainly because of their advantages, such as abundance and negligible cost, whereas non-renewable energy sources are limited due to shortages and high costs [1]. According to the 'Global Energy Review 2021' by 'International Energy Agency', in the current post-pandemic scenario, non-renewable (oil) energy demand rebounded by 3% due to the global vaccination regime; however, it declined by 4% in the year 2020 compared with 2019 [2]. Carbon dioxide (CO_2) emissions and energy demand have increased compared with 2020, surpassing the previous gross domestic product (GDP), with increasing demands on the energy sector; therefore, the COVID-19 pandemic has impacted global energy demand. Developing sustainable and green energy sources is a big challenge for all researchers [3]. Considering all the renewable energy sources, hydrogen (H_2) energy is currently becoming a low-cost, highly appreciable, and sustainable energy source, which can be used to store, move, and deliver the energy produced from other resources [4]. Moreover, carbon-free, sustainable, and eco-friendly H_2 energy generation is an important prerequisite for future economics, and it also acts as the driving force for innovations in the field of renewable energy. William Robert Grove first invented the H_2 fuel cell to store generated hydrogen in the year 1839 [5], establishing

the foundation for future H_2 technology that can store evolved H_2 in its pure form; therefore, researchers worldwide are increasingly considering the advantages and needs of H_2 energy [6–8].

How Can H_2 Be Generated Sustainably and Eco-Friendly?

Renewable energy sources, i.e., wind, biomass, and solar, are used for photocatalytic H_2 generation [9]; however, these sources are regional and seasonal. Therefore, H_2 can be generated by splitting water in H_2 and oxygen (O_2) by using sunlight (photocatalysis) [10], thermal and chemical (thermochemical catalysis) [11], and electrical (electrocatalytic) methods [12]. In addition, being a natural and abundant source of sunlight with no carbon dioxide (CO_2) gas emissions, solar energy is playing a crucial role in overcoming kinetic barriers during heterogeneous catalysis. State-of-the-art methods involve materials where the catalysts possess higher values for solar-driven hydrogen evolution reactions (HER), and they include noble metals, such as pure platinum (Pt), iridium (Ir), and ruthenium (Ru), as well as noble-metal-free photocatalysts. Many reports are available for Pt-based H_2 production using photocatalytic HER due to its high redox activity and zero overpotential [13]. However, the latest report on the approach for avoiding mass transport limitations and achieving the highest turnover frequency (TOF) when using Pt nanoparticles compared with the commercial platinum/carbon (Pt/C) catalysts illustrates that some of the pitfalls for obtaining a high-value TOF relate to measurement issues, such as the need for potential scale calibration, the choice of an incorrect counter electrode, and a lack of H_2 saturation [14] during solar photocatalytic HER. Similarly, as reported by Koo et al., platinum nanocubes synthesized using an aqueous colloidal route exhibited a promising photocurrent density of 1.77 A/mg at −100 mV [15]. Heterogeneous photocatalysis using oxide-based nanomaterials is becoming a pioneering research area, leading to prominent H_2 evolution results both in combination with, and without, noble metals [16–18], with Pt and Pt-group members being used with other inexpensive metal oxides to form alloys [19]. Therefore, Pt is the best catalyst in the field of catalysis to date and has also been explored for H_2 production using wastewater compounds [20]; however, the production of large amounts of H_2 is limited due to the cost of Pt and Pt-based commercial catalysts, high agglomeration rates, poor stability, and low removable efficacy. Low-cost, noble-metal-free photocatalysts are explored by Thakur et.al for efficient H_2 evolution (2531 µmol/g) based on a phosphorus-doped graphitic carbon nitride-P25 (TiO_2) composite and TiO_2/g-C_3N_4/p-g-C_3N_4 nanocomposite [21]. The optical properties of titanium nitride were enhanced using red phosphor, meaning the resulting nanocomposite could evolve the 0.5 µmol/g/h [22] of H_2. Sergei Poskunov et al. designed a novel photocatalyst, for which a single atom of gold, silver, and copper was deposited on the surface of TiO_2, and analyzed its electronic properties using real-time, time-dependent density functional theory (RT-TD-DFT) [23]. Conclusively, the wider research community has explored new emerging magnetic and non-magnetic nanomaterials that are based on noble- and non-noble-metal-based photocatalysts for eco-friendly H_2 generation [23–25].

2. Role of Removable Photocatalysts

Considering the many innovations achieved in the field of solar photocatalytic H_2 evolution, much less attention has been given to the byproducts generated after completing the reaction, which can cause a hazard to the environment [26]. Therefore, the first step towards sustainable and eco-friendly H_2 generation using novel nanomaterials is to find their dissociation mechanism and removal efficacy. Magnetic nano-catalysts such as Fe_2O_3 (hematite) and Fe_3O_4 (maghemite) are prominent and well established, with inherent or non-inherent magnetic properties, which allow them to be easily separated from an aqueous solution. Furthermore, spinel ferrite nanomaterials are novel types of magnetic nanomaterials that can be removed easily after the overall completion of HER. They are composed of an AB_2O_4 formula, where A and B are the divalent and trivalent cations coordinated with negatively charged oxygens or anions. Many compositions of spinel ferrites are possible

due to the Earth's abundance of metals, non-metals, and metalloids. Because nano-sized ferrites are an efficient photocatalyst, they are robust, and are characterized by thermal, chemical, and photostability; ease of production; a small band gap; tunable size; and higher levels of visible light absorption with appropriate positioning of the conduction band (CB) and valence band (VB); therefore, they are considered for photocatalytic HER. However, according to the available literature, until the year 2022, research on spinel ferrites for H_2 production has been limited. In the year 2019, Pu et al. developed a 1D recyclable p-n junction of a nanocomposite based on $CoFe_2O_4/Cd_{0.9}Zn_{0.1}S$, which was separated multiple times from the solution by using a proposed H_2 evolution mechanism [27]. Some other experimental reports are also available for the removal and recovery of ferrite-based nanomaterials [28,29]; however, they are limited and do not meet efficiency criteria compared with well-established nanomaterials, such as porous metal–organic frameworks (MOFs) [30]. Only 7% of publications before 2021 included material separation after the reaction [31]. The ab initio methods, i.e., density function theory (DFT), are extremely useful for understanding and exploring spinel ferrite nanomaterials, especially their fundamental properties related to electronic band structures and charge transfer dynamics/kinetics, as well as their experimental limitations. Using these ab initio methods, we can determine their electronic transitions, which are structures between most of the crystal structures, as well as their tetrahedral and octahedral cations (spinel ferrites) [32]. The structural, elastic, electronic, and thermodynamic properties of spinel ferrites nanomaterials derived using periodic ab initio CRYSTAL14 code based on the LCAO (linear combination of atomic orbitals) method with local Gaussian-type basis sets (BSs) have been reported in detail [33].

3. The Mechanism for H_2 Evolution

The photocatalytic hydrogen evolution reaction (HER) is only possible when the photocatalyst can absorb the energy provided by a light source; this is necessary for the excitation of electrons from the valence band (VB) to the conduction band (CB), a process that leaves behind a hole. Similarly, in the case of spinel ferrites, the absorption of visible light leads to the excitation of electrons from the VB to the CB, which causes a hole formation in the VB, because of their narrow band gap energy values, which are capable of absorbing most of the visible light. Initially, an excited electron in the CB of spinel ferrite contributes to the breaking of bonds in adsorbed H_2O molecules and governs the classic theory called Volmer, Heyrovsky, and Tafel reactions.

The Volmer step contributes to the dissociation of adsorbed water molecules:

$$H_2O + e^- \rightarrow H^* + OH \quad (1)$$

Heyrovsky step and Tafel step contribute to the production of molecular H_2

$$H^* + e^- + H_2O \rightarrow H_2 + OH \quad (2)$$

$$2H^* + 2e^- \rightarrow H_2 \quad (3)$$

Similarly in the case of AB_2O_4 (ferrites) as photocatalysts, the reaction mechanism, it involves,

$$AB_2O_4 + 2H_2O \rightarrow AB_2O_4\text{-}H + H_2O \quad (4)$$

$$AB_2O_4\text{-}H + H_3O + e^- \rightarrow AB_2O_4\text{-}H + H_3O \quad (5)$$

$$H_3O^+ + e^- + AB_2O_4\text{-}H \rightarrow AB_2O_4 + H_2 + H_2O \quad (6)$$

$$AB_2O_4\text{-}H + AB_2O_4\text{-}H \rightarrow 2\,AB_2O_4 + H_2 \quad (7)$$

4. Contributing Factors

Many factors affect H_2 evolution during photocatalysis, and they are discussed extensively with a focus on the development of effective photocatalysts. An illustration of the factors that contribute to H_2 evolution is given in Figure 1.

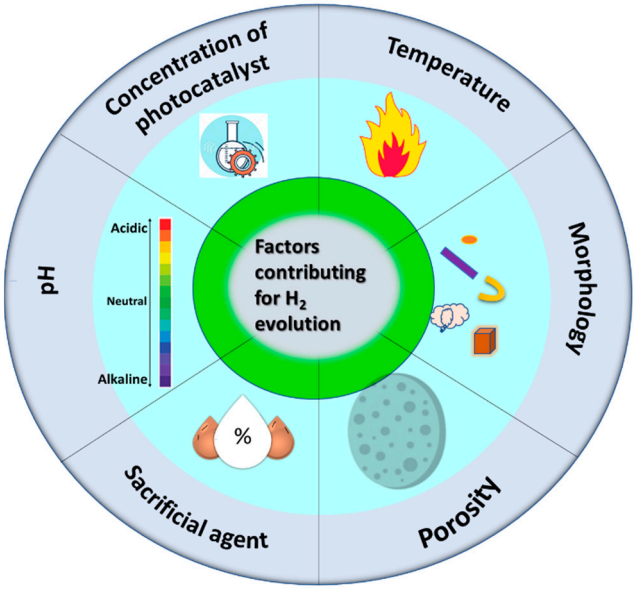

Figure 1. Illustration of different factors contributing to H_2 evolution.

4.1. Morphology

Nanomaterials have high functionality and diverse physicochemical properties that are comprehensively related to their photocatalytic properties [34,35]. Pure and hybrid oxide-based nanomaterials have been employed as efficient photocatalysts for water splitting and can produce and store hydrogen (H_2) following hydrogen evolution reactions (HER). Zero-dimensional (0D) nanomaterials, such as CdS, CdSe, and carbon quantum dots, are employed for visible light H_2 evolution; however, they are limited in efficiency due to their high-corrosion and charge-recombination rates. Addressing this, Li. et al. reported the photo deposition of metal oxides on quantum dots and alleviated the drawbacks [36]. Bimetallic plasmonic nanomaterials such as Ag@Au, i.e., a core–shell structure with an Au core and Ag shell, have emerged as next-generation photocatalysts for H_2 generation [37]. One-dimensional (1D) nanomaterials consist of nanorods (NRs) [38], nanowires (NWs) [39], nanotubes (NTs) [40], and nanofibers (NFs), contributing to their superior properties, which are suitable for photocatalysis for H_2 evolution. Their extremely large surface-to-volume ratio is favorable for photogenerated charge carriers and their ballistic transport. Zn_2GeO_4 is a type of 1D NRs that produces the highest rate of H_2, namely, 0.6 mmol/h in basic conditions [41]. The morphological characteristics of 1D porous [42] TiO_2 NTs are effectively utilized for photocatalytic activity because their inner diameter supports internal reflections of photons and results in a higher photocurrent density. TiO_2 NTs are broadly explored in pure and doped form for solar-based photocatalysis and H_2 generation, where doped TiO_2 NTs can cover the entire solar spectrum, hence increasing the H_2 production efficiency to 17.39 $\mu mol\ h^{-1}\ cm^{-2}$. Carbon NTs and NFs have extraordinary mechanical and thermal stability. Hence, Jong-Beom Baek et al. anchored Ru nanoparticles on multiwalled CNTs (MWCNTs) to provide catalysis-active sites that are capable of H_2 production of 4194 μ mol V^{-1}, which is 15% greater than Pt/C catalysts [43]. Two-dimensional (2D) nanomaterials are basically in the form of thin films that are established for H_2 evolution due to their large surface area compared with zero- and one-dimensional nanomaterials. Because the overall water-splitting phenomenon depends on the amount of light absorbed by the catalysis, and because there is a high chance of recombination of separated charges, scaling up the amount of photocatalyst in aqueous dispersion also affects the rate of H_2

evolution. Therefore, thin-film-based photocatalysts are explored in academia with novel nanomaterials such as transition metal dichalcogenides (TMDs) [44], graphene oxide [45], and graphitic carbon nitride (g-C_3N_4) [46]. The issues regarding the low performance of the catalysis and H_2 evolution in the particulate form are overcome by the deposition of thin films using spin-coating, hydrothermal, chemical bath (CBD), and electrostatic spray pyrolysis (ESP) deposition methods, where the experimental parameters are varied to obtain the perfect VB and CB positions required for water splitting [47]. Thin films of metal oxides such as TiO_2 and Fe_2O_3 showed better H_2 evolution rates than that of the powder formed [48]. The porosity photocatalysts play a vital role in providing the active sites for H_2 production and the water adsorption required for catalysis. The 1D, 2D, and 3D metal–organic frameworks (MOFs) have been widely studied regarding the overall pH range for H_2 evolution reactions, among which 2D MOFs with a sheet-like morphology became high-potential candidates [49,50]. Cobalt dithiolene is one of the best photocatalysts based on the lowest overpotential values for H_2 evolution, which can also be derived from MOFs [51]. Transition-metal-doped MOFs, such as transition metal phosphides (TMPs), are currently trending 2D nanomaterials for heterogeneous catalysis. However, neither the stability of MOFs during the overall water splitting process nor the degradation and removal mechanisms are elaborated upon in the literature; nor are the associated problems and limitations for scaling up H_2 evolution.

4.2. pH and Sacrificial Agents

The acidic pH of the solution contributes to HER, where the H^+ ion concentration is high. Diluted acid such as hydrogen sulfate (H_2SO_4) is used for providing acidic conditions. However, hole scavengers, such as ethanol and methanol/glycerol reaction media, have a basic pH. Different types of scavengers such as methanol, glycerol, formic acid, lactic acid, ethylenediamine (EDTA), triethanolamine, and sodium sulfate (Na_2SO_4) assist in controlling the charge recombination rate. Likuta et al. have undertaken a kinetic study of pH dependent H_2 production [52]. The hydrogen ion concentration or protons are known as the pH of the solution, which also affects the other chemical interactions among the catalyst and substrate during photocatalysis, such as adsorption and the agglomeration of particulates. The greater aggregation, the more the photocatalyst will be sedimented, with more effort needed for their stable suspension. Essentially, measurements of H_2 evolution are carried out in an environment where the dissociation of the photocatalyst without light is prevented, with the medium acting as a hole scavenger. Therefore, H_2 evolution also depends on the concentration of the sacrificial agent used during photocatalysis, where the stability of photocatalysts plays a considerable role [53].

4.3. Temperature

Temperature is a key factor that contributes to an increased rate of H_2 evolution. Recently, an increased rate of about 38.0 $mmol \cdot g^{-1}$ h^{-1} at 60 °C was achieved by Núñez et al. via HER, two times greater than room temperature [54]. The catalytic performance of TiO_2 nanoparticles can also be enhanced by deposition on the SiO_2 substrate, thereby increasing the temperature of the water-splitting reaction and lowering the overpotential and reaction time [55]. The temperature of the photocatalytic reaction setup can also be increased automatically via a high-energy sunlight source. Collectively, the elevated temperature causes an increased rate of carrier mobility and effective charge transfer during visible light photocatalysis. After a certain saturation temperature, the activity can be decreased depending on the stability of the photocatalyst at higher temperatures and carrier recombination. Therefore, the temperature range is optimized for each different nanomaterial. Achieving high photocatalytic activity is a crucial challenge and using transition-metal-based oxide materials is favorable. Moreover, Xu and Li. et al. synthesized graphitic carbon nitride (g-C_3N_4)-layered microstructures combined with a Pt co-catalyst, with which they could obtain a H_2 evolution of 800 μmol^{-1} g^{-1} at a lower temperature (10 °C) [56].

4.4. Concentration of Photocatalyst

An aqueous solution of a particulate-form photocatalyst should be prepared such that an optimal surface will be available to water molecules for an adsorption phenomenon called chemisorption. The higher the concentration of the photocatalyst, the more the adsorption of water molecules takes place, and the higher the rate of H_2 evolution. The effect of varied concentrations of copper/zinc sulfide/$CoFe_2O_4$ (Cu/ZnS/COF) core–shell photocatalysts with 0.1 g/L to 0.6 g/L was studied by Wu et al. They observed that 0.3 g/L was the optimal concentration, where the maximum H_2 evolution was observed and then decreased [55].

Table 1 illustrates the contributing factors, such as temperature, pH, sacrificial agent, and amount/concentration of photocatalysts, on photocatalytic H_2 evolution via spinel ferrite nanomaterials. Most of the HER are feasible at room temperature; however, an increase in the reaction temperature to 50 °C is needed for some photocatalysts. Considering the pH of the medium, HER are favorable for acidic media, where the reports also suggest that, with an appropriate sacrificial agent, the H_2 evolution rate could be increased at a basic pH compared with an acidic or neutral pH [57]. Similarly, the effect of dosage/concentration of photocatalysts on H_2 evolution showed that optimal concentration needs to be checked during the experiments. However, the presence of sacrificial agents increased the rate of H_2 evolution compared with the medium containing no sacrificial agent.

Table 1. Factors contributing to H_2 evolution based on spinel ferrites photocatalysts.

Spinel Ferrite Photocatalyst	Temperature (°C)	Concentration of Photocatalyst (g L^{-1})	pH	Sacrificial Agent	Amount of H_2 Produced (μmol^{-1} g^{-1})	Ref.
$CoFe_2O_4/ZnIn_2S_4$	25	0.5	Basic	Triethanolamine	800	[58]
1. $CuFe_2O_4$ 2. $NiFe_2O_4$	25	0.5	Acidic	With no Sacrificial agent With Na_2SO_3 and Na_2S	336 and 234 1.3605 2.3171	[59]
$CuFe_2O_4$/ TiO_2	50	1	Neutral 13	$Na_2SO_4/Na_2S_2O_3$ KOH	80 170	[60]
$CuFe_2O_4/g\text{-}C_3N_4$	25	1	Acidic Basic	Na_2SO_4 Triethanolamine	200 700	[57]
Pr_2NiO_4/SnO_2	50	1	Neutral 12	$Na_2S_2O_3$ KOH	276 146	[61]
$Ag/NiFe_2O_4$	50	1	>7	KOH	123	[62]
$ZnFe_2O_4$	25	0.01	-	-	133.5	[63]
$g\text{-}C_3N_4/BiVO_4/CoFe_2O_4$	25	-	Basic	EDTA	-	[64]
$Ag_2CrO_4/GO/MnFe_2O_4$	25	Thin film	Acidic	Na_2SO_4	446.93	[65]
Cu/ZnS/COF	25	0.1 0.2 0.3 0.4 0.5 0.6	Acidic	Formic acid	30 125 278 175 174 100	[55]

5. Synthesis Approaches

The process of H_2 evolution is generally carried out with a particulate or thin films (anode/cathode) as photocatalysts. In particulate-form H_2 production, an amount of the powder-form photocatalyst is subjected to solar power while being continuously stirred; the thin-film forms of the photocatalysts are prepared by depositing them on the conducting substrate before they are placed in a hanging condition in the reactor vessel/tube. Particulate-form H_2 production limits the solar-to-hydrogen (STH) efficiency due to the scattering effects being larger than absorption, the small surface area, and the increased charge recombination, although factors limiting the efficiency of oxide-based thin films

include the lack of composition of different types of oxide materials, enhancing charge diffusion and separation to actual redox sites. Cobalt and nickel ferrite-based graphene nanocomposites are well explored, and their electrochemical performance showed their aptness for HER [66]. Thin-film deposition methods for spinel ferrites as solar-based photocatalysts include spin coating, spray coating, vacuum deposition, laser deposition, and sputtering, where the particulate from spinel ferrites can be synthesized using the sol–gel method, hydrothermal method, ball milling, etc. Many other researchers reported the synthesis of thin films using chemical methods of synthesis, as shown in Table 2. These methods also limit the uniform deposition and adherent thin films compared with physical methods of deposition. The properties of photocatalysts also depend on the synthesis condition or deposition technique, and in the case of TiO_2, the phase varies with the chemical and physical deposition technique of the thin film and holds different strengths and weaknesses. Chemical deposition methods for thin films include successive ionic layer adsorption and reaction (SILAR), hydrothermal coating, electrodeposition, electrospinning, etc. These methods can deposit thin films with different morphologies with proper optimization steps at a low cost. Spinel ferrite Co-$ZnFe_2O_4$ thin-film nanostructures developed using hydrothermal reactions possess good photocatalytic activity and could produce H_2 with 0.0088 μmol/cm^2 min. Chen et al. synthesized CdS-sensitized $ZnFe_2O_4/ZnIn_2S_4$ nanosheets using ionic layer adsorption reactions and could evolute the H_2 by about 79 μmol/h. Moreover, the physicochemical properties of spinel ferrites are sensitive to the synthesis strategies because transition and non-transition ions possess different oxidation states, which consequently lead to normal and inverse spinel structures. Normal spinel is a type of ferrite where A and B sites form complete tetrahedral and octahedral coordination with metal ions, respectively, e.g., i = 1, and for the inverse spinel inversion degree, i = 0–1. An A site ion has comparably smaller Shannon ionic radii than a B site and can develop a number of combinations depending on the application required. Moreover, maintaining stoichiometry is the most crucial task for obtaining the desired phases of ferrite nanomaterials. Researchers have reported different types of physical, chemical, and biological methods for the synthesis of spinel ferrites.

Table 2 elaborates on the synthesis strategies reported in the years 2010–2022, the morphology and amount of H_2-generated ferrite-based catalysts, and some co-catalysts thereof. The need for porous spinel ferrite nanostructures for enhanced efficiency of H_2 generation and CO_2 reduction is also fulfilled by many researchers. Xiaoxing Xu et al. reported enhanced H_2 performance with Ga-doped $ZnFe_2O_4$, where Ga doping created trap states between the energy levels, hence increasing charge migration and band gap energy compared with the parent $ZnFe_2O_4$ [67]. There is a strong correlation between catalytic activity and crystal structures along with all the physicochemical properties [68]. Moreover, the high-temperature calcination required for the pure-phase formation of spinel ferrite can eliminate the trapping sites for electrons and holes and hence can be avoided to decrease the recombination rates. Interestingly, the size of magnetic nanomaterials plays a very important role in the determination of their magnetic properties, and after a certain critical size, they become superparamagnetic and single-domain particles that are important for the easy removal of ferrite nanoparticles after H_2 evolution in an aqueous medium. Figure 2 illustrates (a) the synthesis methods of ferrite nanomaterials as elaborated in Table 2; (b) their mechanism for solar-based H_2 evolution as explained previously in Section 3; (c) removal and recyclability; and (d) applications for fuel cell technology.

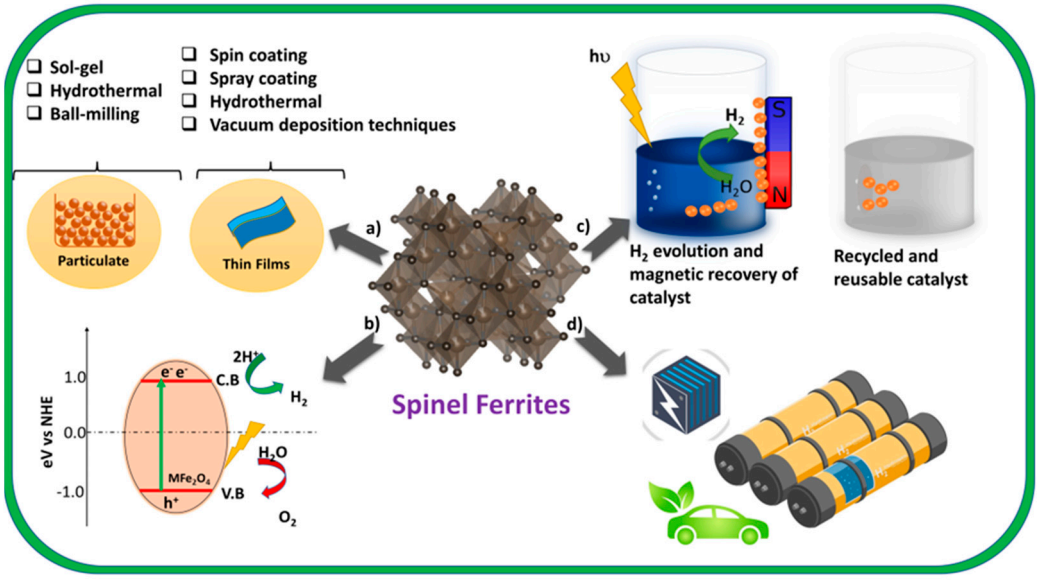

Figure 2. Showing (**a**) methods for the synthesis of particulate and thin films of ferrite nanomaterials (**b**) mechanism of H_2 evolution (**c**) removal and recycling of ferrite photocatalysts (**d**) applications of H_2 energy of vehicles and fuel cells.

Table 2. Available literature for spinel ferrites photocatalysts.

Year of Publishing	Photocatalyst	Synthesis Method	Morphology and Particle Size (nm) Obtained	Amount of H_2 Evolved	Light Intensity	Ref.
2011	$Co_{0.85}Fe_{2.15}O_4$	Atomic Layer deposition	Non-uniform spheres of <10	40 µmol/S/g		[69]
2012	Fe_3O_4	Co-Precipitation	10 Spherical	8275 µmol/h/g	400 W	[18]
2012	$ZnFe_2O_4$	Microwave irradiation method	Agglomerated spheres of 50 nm	133.5 µmol/g	300 W	[63]
2012	$NiFe_2O_4$	Co-precipitation	17.8 nm Agglomerated particles	15.45 µmol/g	250 W	[70]
2012	1. CO_3O_4 2. Fe_3O_4	Sol-Gel	12.42 nm Coral like	(1) 2000 µmol/h/g (2) 8275 µmol/h/g	200 W	[71]
2013	1. $ZnFe_2O_4$ 2. $ZnFe_2O_4$:Fe_2O_3	Plasma Spraying	>10 nm Porous spherical	(1) 46.3 µmol/h (2) 99 µmol/h	1000 W/m^2	[72]
2013	$CuFe_2O_4$/g-C_3N_4 with Pt catalyst	Sol-gel	15–25 nm Particles on g-C_3N_4 sheets	76 µmol/h	300 W	[73]
2013	$NiFe_2O_4$@TiO_2	Sol-gel	100–300 nm Spherical	18.5 mL	18 W/cm^2	[74]
2014	$CaFe_2O_4$/TiO_2	Sol-Gel	1–2 µm Spherical	2111 µmol/h/g	-	[75]
2014	$NiFe_2O_4$	Aerosol Spray Pyrolysis	11 nm Spherical porous	0.09 µmol h^{-1}	-	[76]
2015	$CoFe_2O_4$	Co-precipitation and ball milling	25 nm Agglomerates	2540 and 3490 µmol/g	250 W	[77]
2015	$ZnFe_2O_4$	Microwave synthesis	35 nm Porous spheres	218 µmol/h/g	AM 1.5 G (1000 W/m^2)	[78]

Table 2. *Cont.*

Year of Publishing	Photocatalyst	Synthesis Method	Morphology and Particle Size (nm) Obtained	Amount of H_2 Evolved	Light Intensity	Ref.
2015	1. g-C_3N_4-$CoFe_2O_4$ 2. g-C_3N_4-$NiFe_2O_4$	Modified Sol-gel method	67 & 54 nm Irregular shape	1.55 and 1.24 µmol/g	300 W	[28]
2016	1. $ZnFe_2O_4$ 2. $Cu0.2Zn0.8Fe_2O_4$ 3. $Co0.2Zn0.8Fe_2O_4$ 4. $Ni0.2Zn0.8Fe_2O_4$	Co-precipitation	27 nm 20 nm 18 nm 12 nm	(1) 195 µmol g^{-1} s^{-1} (2) 9 µmol g^{-1} s^{-1} (3) 675 µmol g^{-1} s^{-1} (4) 233 µmol g^{-1} s^{-1}	200 W	[79]
2017	S-$NiFe_2O_4$	Electrodeposition	2 nm Porous nanoflakes	-	-	[80]
2019	$CoFe_2O_4/Cd_{0.9}Zn_{0.1}S$	Hydrothermal	20 nm Nanorods	350.2 µmol/h	AM 1.5 G	[27]
2020	$FeSe_2/CoFe_2O_4$	Hydrothermal	100 nm rods	-	-	[81]

6. Conclusions and Future Prospects

To summarize the present work, we have reviewed synthesis approaches for spinel ferrites, factors contributing to H_2 evolution, and their need for recoverable and robust photocatalysts. The synthesis techniques for achieving pure phase and good inherent magnetization need calcination processes that lead to low dispersity; therefore, alternative methods for achieving excellent colloidal stability in the desired phase are yet to be explored. The dissociation or stability of spinel ferrite in acidic or basic media is also not yet explored, which should be taken into consideration. H_2 evolution using ferrite-based nanomaterials is quite possible at room temperature; however, at elevated temperatures, a study should be carried out for their phase stability and crystallinity because the magnetic properties of spinel ferrites depend on temperature. The choice of a good sacrificial agent for avoiding charge recombination is needed where it can be optimized for ferrite-based nanomaterials. One possible strategy to improve H_2 evolution is to improve active sites on spinel ferrites with the design and development of composite nanomaterials and to understand their VB and CB position. Optical properties can be tuned by changing the oxygen concentration and narrowing the band gap of ferrite nanomaterials for greater visible light absorption. Computational analysis can be introduced for the predefined tuning of band gaps using DFT techniques so that the required band edges can be easily inserted in the spinel ferrites required for trapping the electrons during H_2 evolution. A novel strategy can be developed based on spinel ferrites–red phosphor (RP) nanocomposites because red phosphors are capable of solar energy harvesting with a band gap of 1.8 eV [22]. Spinel ferrites have a wide optical bandgap and can be combined with different transition and rare-earth elements to be used as phosphors in HER [33]. However, we can use the magnetic ferrite nanomaterials for visible light HER after their successful removal with an external magnetic field, and more efforts should be expended to develop a suitable set-up. On the other hand, Pt/Ir/Ru are the most effective catalysts, and the cost of industry scale-up can be minimized with the development of Pt/Ir/Ru-spinel ferrite nanocomposites for H_2 evolution. After the removal of the catalyst, the reusability of the photocatalyst can be checked, which will need successive characterizations. The present overview describing all the aspects of spinel ferrite nanomaterials will be beneficial for the next generation photocatalysts for H_2 evolution reactions and could open new routes for their future applications, such as in fuel cells, which are the best photocatalysts. We strongly believe that addressing these research gaps will help to develop efficient, effective, and highly stable, low-cost ferrite-based photocatalysts for sustainable H_2 generation and utilization.

Author Contributions: Conceptualization, Y.J. and A.K.; methodology, A.K.; resources, A.K.; data curation, S.W.; writing—original draft preparation, S.W. and Y.J.; writing—review and editing, Y.J. and A.K.; All authors have read and agreed to the published version of the manuscript.

Funding: The author (A.K.) is grateful to Symbiosis International University (SIU) for providing Research Support Fund (RSF).

Data Availability Statement: Data will be made available on request by corresponding authors.

Conflicts of Interest: The authors have no relevant competing interests.

Abbreviations

Ag@Au	A core-shell structure with the Au core and Ag shell
CdS	Cadmium Sulfide
CdSe	Cadmium Selenide
CO_2	Carbon Dioxide
COVID-19	Coronavirus Disease of 2019
GDP	Gross Domestic Product
H_2	Hydrogen
Ir	Iridium
NRs	Nanorods
NWs & NTs	Nanowires & Nanotubes
RP	Red Phosphor
TiO_2/g-C_3N_4/p-g-C_3N_4	metal-free phosphorus doped graphitic carbon nitride-P25 (TiO_2) nanocomposite

References

1. Halkos, G.E.; Gkampoura, E.-C. Reviewing Usage, Potentials, and Limitations of Renewable Energy Sources. *Energies* **2020**, *13*, 2096. [CrossRef]
2. Newell, R.; Raimi, D.; Villanueva, S.; Prest, B. *Global Energy Outlook 2021: Pathways from Paris*; Resources for the future: Washington, DC, USA, 2021; Volume 8.
3. Eroglu, H. Effects of COVID-19 outbreak on environment and renewable energy sector. *Environ. Dev. Sustain.* **2021**, *23*, 4782–4790. [CrossRef]
4. Farias, C.B.B.; Barreiros, R.C.S.; da Silva, M.F.; Casazza, A.A.; Converti, A.; Sarubbo, L.A. Use of Hydrogen as Fuel: A Trend of the 21st Century. *Energies* **2022**, *15*, 311. [CrossRef]
5. Perry, M.L.; Fuller, T.F. A historical perspective of fuel cell technology in the 20th century. *J. Electrochem. Soc.* **2002**, *149*, S59.
6. Andrei, V.; Ucoski, G.M.; Pornrungroj, C.; Uswachoke, C.; Wang, Q.; Achilleos, D.S.; Kasap, H.; Sokol, K.P.; Jagt, R.A.; Lu, H.; et al. Floating perovskite-BiVO4 devices for scalable solar fuel production. *Nature* **2022**, *608*, 518–522. [CrossRef]
7. Mahmood, N.; Yao, Y.; Zhang, J.W.; Pan, L.; Zhang, X.; Zou, J.J. Electrocatalysts for Hydrogen Evolution in Alkaline Electrolytes: Mechanisms, Challenges, and Prospective Solutions. *Adv. Sci.* **2018**, *5*, 1700464. [CrossRef]
8. Zheng, Y.; Jiao, Y.; Zhu, Y.; Li, L.H.; Han, Y.; Chen, Y.; Du, A.; Jaroniec, M.; Qiao, S.Z. Hydrogen evolution by a metal-free electrocatalyst. *Nat. Commun.* **2014**, *5*, 3783. [CrossRef]
9. Jawhari, A.H.; Hasan, N.; Radini, I.A.; Malik, M.A.; Narasimharao, K. Pt-Ag/Ag_3PO_4-WO_3 nanocomposites for photocatalytic H_2 production from bioethanol. *Fuel* **2023**, *344*, 127998. [CrossRef]
10. Jafari, T.; Moharreri, E.; Amin, A.S.; Miao, R.; Song, W.; Suib, S.L. Photocatalytic Water Splitting—The Untamed Dream: A Review of Recent Advances. *Molecules* **2016**, *21*, 900. [CrossRef] [PubMed]
11. Rao, C.N.; Lingampalli, S.R.; Dey, S.; Roy, A. Solar photochemical and thermochemical splitting of water. *Philos. Trans. A Math. Phys. Eng. Sci.* **2016**, *374*, 20150088. [CrossRef]
12. Li, J.; Hu, J.; Zhang, M.; Gou, W.; Zhang, S.; Chen, Z.; Qu, Y.; Ma, Y. A fundamental viewpoint on the hydrogen spillover phenomenon of electrocatalytic hydrogen evolution. *Nat. Commun.* **2021**, *12*, 3502. [CrossRef]
13. Verma, S.; Sinha-Ray, S.; Sinha-Ray, S. Electrospun CNF Supported Ceramics as Electrochemical Catalysts for Water Splitting and Fuel Cell: A Review. *Polymers* **2020**, *12*, 238. [CrossRef]
14. Hansen, J.N.; Prats, H.; Toudahl, K.K.; Morch Secher, N.; Chan, K.; Kibsgaard, J.; Chorkendorff, I. Is There Anything Better than Pt for HER? *ACS Energy Lett.* **2021**, *6*, 1175–1180. [CrossRef] [PubMed]
15. Koo, B.; Chu, J.; Seo, J.; Jung, G.; Baek, S.H.; Nam, S.W.; Duah, C.; Lee, Y.K.; Jung, W.; Shin, B.J.C. Drop-casted Platinum Nanocube Catalysts for Hydrogen Evolution Reaction with Ultrahigh Mass Activity. *ChemSusChem* **2021**, *14*, 2585–2590. [CrossRef] [PubMed]
16. Dahanayake, A.; Gunathilake, C.A.; Pallegedara, A.; Jayasinghe, P. Recent Developments in Noble Metal-Free Catalysts for a Photocatalytic Water Splitting Process—A Review. *J. Compos. Sci.* **2023**, *7*, 64. [CrossRef]

17. Li, C.; Baek, J.B. Recent Advances in Noble Metal (Pt, Ru, and Ir)-Based Electrocatalysts for Efficient Hydrogen Evolution Reaction. *ACS Omega* **2020**, *5*, 31–40. [CrossRef]
18. Jawhari, A.H.; Hasan, N.; Radini, I.A.; Narasimharao, K.; Malik, M.A. Noble Metals Deposited $LaMnO_3$ Nanocomposites for Photocatalytic H_2 Production. *Nanomaterials* **2022**, *12*, 2985. [CrossRef]
19. Mangrulkar, P.A.; Polshettiwar, V.; Labhsetwar, N.K.; Varma, R.S.; Rayalu, S.S. Nano-ferrites for water splitting: Unprecedented high photocatalytic hydrogen production under visible light. *Nanoscale* **2012**, *4*, 5202–5209. [CrossRef]
20. Rioja-Cabanillas, A.; Valdesueiro, D.; Fernández-Ibáñez, P.; Byrne, J.A. Hydrogen from wastewater by photocatalytic and photoelectrochemical treatment. *J. Phys. Energy* **2020**, *3*, 012006. [CrossRef]
21. Wadhai, S.; Jadhav, Y.; Thakur, P. Synthesis of metal-free phosphorus doped graphitic carbon nitride-P25 (TiO_2) composite: Characterization, cyclic voltammetry and photocatalytic hydrogen evolution. *Sol. Energy Mater. Sol. Cells* **2021**, *223*, 110958. [CrossRef]
22. Raykar, V.S.; Patil, S.B.; Patil, P.S. *Porous TiN/Red Phosphorus Nanocomposite for Photocatalytic Hydrogen Evolution*; Macromolecular Symposia, 2020; Wiley Online Library: Hoboken, NJ, USA, 2020; p. 2000003.
23. Lin, Y.-P.; Bocharov, D.; Kotomin, E.A.; Brik, M.G.; Piskunov, S.J. Influence of Au, Ag, and Cu Adatoms on Optical Properties of TiO_2 (110) Surface: Predictions from RT-TDDFT Calculations. *Crystals* **2022**, *12*, 452. [CrossRef]
24. Wei, X.; Naraginti, S.; Yang, X.; Xu, X.; Li, J.; Sun, J.; Liu, Z.; Pei, J. A novel magnetic $AgVO_3$/rGO/$CuFe_2O_4$ hybrid catalyst for efficient hydrogen evolution and photocatalytic degradation. *Environ. Res.* **2023**, *229*, 115948. [CrossRef] [PubMed]
25. Kumar, S.; Kumar, A.; Navakoteswara Rao, V.; Kumar, A.; Shankar, M.V.; Krishnan, V. Defect-Rich MoS_2 Ultrathin Nanosheets-Coated Nitrogen-Doped ZnO Nanorod Heterostructures: An Insight into in-Situ-Generated ZnS for Enhanced Photocatalytic Hydrogen Evolution. *ACS Appl. Energy Mater.* **2019**, *2*, 5622–5634. [CrossRef]
26. Najaf, Z.; Nguyen, D.L.T.; Chae, S.Y.; Joo, O.-S.; Shah, A.U.H.A.; Vo, D.-V.N.; Nguyen, V.-H.; Le, Q.V.; Rahman, G. Recent trends in development of hematite (α-Fe_2O_3) as an efficient photoanode for enhancement of photoelectrochemical hydrogen production by solar water splitting. *Int. J. Hydrogen Energy* **2021**, *46*, 23334–23357. [CrossRef]
27. Shao, Z.; Zeng, T.; He, Y.; Zhang, D.; Pu, X. A novel magnetically separable $CoFe_2O_4$/$Cd_{0.9}Zn_{0.1}S$ photocatalyst with remarkably enhanced H_2 evolution activity under visible light irradiation. *Chem. Eng. J.* **2019**, *359*, 485–495. [CrossRef]
28. Chen, J.; Zhao, D.; Diao, Z.; Wang, M.; Shen, S. Ferrites boosting photocatalytic hydrogen evolution over graphitic carbon nitride: A case study of (Co, Ni)Fe_2O_4 modification. *Sci. Bull.* **2016**, *61*, 292–301. [CrossRef]
29. Chang, C.-J.; Lee, Z.; Chu, K.-W.; Wei, Y.-H. $CoFe_2O_4$@ ZnS core–shell spheres as magnetically recyclable photocatalysts for hydrogen production. *J. Taiwan Inst. Chem. Eng.* **2016**, *66*, 386–393. [CrossRef]
30. Zaman, N.; Noor, T.; Iqbal, N. Recent advances in the metal–organic framework-based electrocatalysts for the hydrogen evolution reaction in water splitting: A review. *RSC Adv.* **2021**, *11*, 21904–21925. [CrossRef] [PubMed]
31. Bielan, Z.; Dudziak, S.; Kubiak, A.; Kowalska, E. Application of spinel and hexagonal ferrites in heterogeneous photocatalysis. *Appl. Sci.* **2021**, *11*, 10160. [CrossRef]
32. Granone, L.I.; Ulpe, A.C.; Robben, L.; Klimke, S.; Jahns, M.; Renz, F.; Gesing, T.M.; Bredow, T.; Dillert, R.; Bahnemann, D.W. Effect of the degree of inversion on optical properties of spinel $ZnFe_2O_4$. *Phys. Chem. Chem. Phys.* **2018**, *20*, 28267–28278. [CrossRef]
33. Brik, M.G.; Ma, C.-G.; Yamamoto, T.; Piasecki, M.; Popov, A.I. First-Principles Methods as a Powerful Tool for Fundamental and Applied Research in the Field of Optical Materials. In *Phosphor Handbook*; CRC Press: Boca Raton, FL, USA, 2022; pp. 1–26.
34. Adán, C.; Marugán, J.; Sánchez, E.; Pablos, C.; van Grieken, R. Understanding the effect of morphology on the photocatalytic activity of TiO_2 nanotube array electrodes. *Electrochim. Acta* **2016**, *191*, 521–529. [CrossRef]
35. Wei, Z.; Mogan, T.R.; Wang, K.; Janczarek, M.; Kowalska, E. Morphology-Governed Performance of Multi-Dimensional Photocatalysts for Hydrogen Generation. *Energies* **2021**, *14*, 7223. [CrossRef]
36. Zhuge, K.; Chen, Z.; Yang, Y.; Wang, J.; Shi, Y.; Li, Z. In-suit photodeposition of MoS_2 onto CdS quantum dots for efficient photocatalytic H_2 evolution. *Appl. Surf. Sci.* **2021**, *539*, 148234. [CrossRef]
37. Ezendam, S.; Herran, M.; Nan, L.; Gruber, C.; Kang, Y.; Gröbmeyer, F.; Lin, R.; Gargiulo, J.; Sousa-Castillo, A.; Cortés, E. Hybrid plasmonic nanomaterials for hydrogen generation and carbon dioxide reduction. *ACS Energy Lett.* **2022**, *7*, 778–815. [CrossRef] [PubMed]
38. Lee, H.; Reddy, D.A.; Kim, Y.; Chun, S.Y.; Ma, R.; Kumar, D.P.; Song, J.K.; Kim, T.K. Drastic Improvement of 1D-CdS Solar-Driven Photocatalytic Hydrogen Evolution Rate by Integrating with NiFe Layered Double Hydroxide Nanosheets Synthesized by Liquid-Phase Pulsed-Laser Ablation. *ACS Sustain. Chem. Eng.* **2018**, *6*, 16734–16743. [CrossRef]
39. Galdámez-Martínez, A.; Bai, Y.; Santana, G.; Sprick, R.S.; Dutt, A. Photocatalytic hydrogen production performance of 1-D ZnO nanostructures: Role of structural properties. *Int. J. Hydrogen Energy* **2020**, *45*, 31942–31951. [CrossRef]
40. Ge, M.; Li, Q.; Cao, C.; Huang, J.; Li, S.; Zhang, S.; Chen, Z.; Zhang, K.; Al-Deyab, S.S.; Lai, Y. One-dimensional TiO_2 Nanotube Photocatalysts for Solar Water Splitting. *Adv. Sci.* **2017**, *4*, 1600152. [CrossRef]
41. Liang, J.; Xu, J.; Gu, Q.; Zhou, Y.; Huang, C.; Lin, H.; Wang, X. A novel Zn_2GeO_4 superstructure for effective photocatalytic hydrogen generation. *J. Mater. Chem. A* **2013**, *1*, 7798–7805. [CrossRef]
42. Qin, N.; Xiong, J.; Liang, R.; Liu, Y.; Zhang, S.; Li, Y.; Li, Z.; Wu, L. Highly efficient photocatalytic H_2 evolution over MoS_2/CdS-TiO_2 nanofibers prepared by an electrospinning mediated photodeposition method. *Appl. Catal. B Environ.* **2017**, *202*, 374–380. [CrossRef]

43. Kweon, D.H.; Okyay, M.S.; Kim, S.J.; Jeon, J.P.; Noh, H.J.; Park, N.; Mahmood, J.; Baek, J.B. Ruthenium anchored on carbon nanotube electrocatalyst for hydrogen production with enhanced Faradaic efficiency. *Nat. Commun.* **2020**, *11*, 1278. [CrossRef]
44. Bozheyev, F.; Ellmer, K.J. Thin film transition metal dichalcogenide hotoelectrodes for solar hydrogen evolution: A review. *J. Mater. Chem. A* **2022**, *10*, 9327–9347. [CrossRef]
45. Sim, Y.; John, J.; Moon, J.; Sim, U. Photo-Assisted Hydrogen Evolution with Reduced Graphene Oxide Catalyst on Silicon Nanowire Photocathode. *Appl. Sci.* **2018**, *8*, 2046. [CrossRef]
46. Zhu, Q.; Xu, Z.; Qiu, B.; Xing, M.; Zhang, J. Emerging Cocatalysts on g-C_3N_4 for Photocatalytic Hydrogen Evolution. *Small* **2021**, *17*, e2101070. [CrossRef]
47. Gaikwad, R.S.; Chae, S.-Y.; Mane, R.S.; Han, S.-H.; Joo, O.-S. Cobalt Ferrite Nanocrystallites for Sustainable Hydrogen Production Application. *Int. J. Electrochem.* **2011**, *2011*, 729141. [CrossRef]
48. Shwetharani, R.; Chandan, H.R.; Sakar, M.; Balakrishna, G.R.; Reddy, K.R.; Raghu, A.V. Photocatalytic semiconductor thin films for hydrogen production and environmental applications. *Int. J. Hydrogen Energy* **2020**, *45*, 18289–18308. [CrossRef]
49. Sun, Y.; Xue, Z.; Liu, Q.; Jia, Y.; Li, Y.; Liu, K.; Lin, Y.; Liu, M.; Li, G.; Su, C.Y. Modulating electronic structure of metal-organic frameworks by introducing atomically dispersed Ru for efficient hydrogen evolution. *Nat. Commun.* **2021**, *12*, 1369. [CrossRef] [PubMed]
50. Wang, J.; Zhang, J.; Peh, S.B.; Zhai, L.; Ying, Y.; Liu, G.; Cheng, Y.; Zhao, D. Dimensional Impact of Metal–Organic Frameworks in Catalyzing Photoinduced Hydrogen Evolution and Cyanosilylation Reactions. *ACS Appl. Energy Mater.* **2018**, *2*, 298–304. [CrossRef]
51. Solis, B.H.; Hammes-Schiffer, S. Computational study of anomalous reduction potentials for hydrogen evolution catalyzed by cobalt dithiolene complexes. *J. Am. Chem. Soc.* **2012**, *134*, 15253–15256. [CrossRef] [PubMed]
52. Karimi Estahbanati, M.R.; Mahinpey, N.; Feilizadeh, M.; Attar, F.; Iliuta, M.C. Kinetic study of the effects of pH on the photocatalytic hydrogen production from alcohols. *Int. J. Hydrogen Energy* **2019**, *44*, 32030–32041. [CrossRef]
53. Velázquez, J.J.; Fernández-González, R.; Díaz, L.; Pulido Melián, E.; Rodríguez, V.D.; Núñez, P. Effect of reaction temperature and sacrificial agent on the photocatalytic H_2-production of Pt-TiO_2. *J. Alloys Compd.* **2017**, *721*, 405–410. [CrossRef]
54. Han, B.; Hu, Y.H. Highly efficient temperature-induced visible light photocatalytic hydrogen production from water. *J. Phys. Chem. C* **2015**, *119*, 18927–18934. [CrossRef]
55. Wang, W.; Li, B.; Yang, H.-J.; Liu, Y.; Gurusamy, L.; Karuppasamy, L.; Wu, J.J. Photocatalytic Hydrogen Evolution from Water Splitting Using Core-Shell Structured Cu/ZnS/COF Composites. *Nanomaterials* **2021**, *11*, 3380. [CrossRef]
56. Huang, S.; Ge, F.; Yan, J.; Li, H.; Zhu, X.; Xu, Y.; Xu, H.; Li, H. Synthesis of carbon nitride in moist environments: A defect engineering strategy toward superior photocatalytic hydrogen evolution reaction. *J. Energy Chem.* **2021**, *54*, 403–413. [CrossRef]
57. Mehtab, A.; Banerjee, S.; Mao, Y.; Ahmad, T. Type-II $CuFe_2O_4$/graphitic carbon nitride heterojunctions for high-efficiency photocatalytic and electrocatalytic hydrogen generation. *ACS Appl. Mater. Interfaces* **2022**, *14*, 44317–44329. [CrossRef]
58. Li, C.; Che, H.; Huo, P.; Yan, Y.; Liu, C.; Dong, H. Confinement of ultrasmall CoFe2O4 nanoparticles in hierarchical $ZnIn_2S_4$ microspheres with enhanced interfacial charge separation for photocatalytic H2 evolution. *J. Colloid Interface Sci.* **2021**, *581*, 764–773. [CrossRef]
59. Soto-Arreola, A.; Huerta-Flores, A.M.; Mora-Hernández, J.; Torres-Martínez, L.M. Comparative study of the photocatalytic activity for hydrogen evolution of MFe_2O_4 (M = Cu, Ni) prepared by three different methods. *J. Photochem. Photobiol. A Chem.* **2018**, *357*, 20–29. [CrossRef]
60. Kezzim, A.; Nasrallah, N.; Abdi, A.; Trari, M. Management, Visible light induced hydrogen on the novel hetero-system $CuFe_2O_4$/TiO_2. *Energy Convers. Manag.* **2011**, *52*, 2800–2806. [CrossRef]
61. Benamira, M.; Lahmar, H.; Messaadia, L.; Rekhila, G.; Akika, F.-Z.; Himrane, M.; Trari, M. Hydrogen production on the new hetero-system Pr_2NiO_4/SnO_2 under visible light irradiation. *Int. J. Hydrogen Energy* **2020**, *45*, 1719–1728.
62. Boukhemikhem, Z.; Brahimi, R.; Rekhila, G.; Fortas, G.; Boudjellal, L.; Trari, M. The photocatalytic hydrogen formation and NO2− oxidation on the hetero-junction Ag/$NiFe_2O_4$ prepared by chemical route. *Renew. Energy* **2020**, *145*, 2615–2620. [CrossRef]
63. Dom, R.; Subasri, R.; Hebalkar, N.Y.; Chary, A.S.; Borse, P.H. Synthesis of a hydrogen producing nanocrystalline $ZnFe_2O_4$ visible light photocatalyst using a rapid microwave irradiation method. *RSC Adv.* **2012**, *2*, 12782–12791. [CrossRef]
64. Yu, F.; Gong, F.; Yang, Q.; Wang, Y. Fabrication of a magnetic retrievable dual Z-scheme g-C_3N_4/$BiVO_4$/$CoFe_2O_4$ composite photocatalyst with significantly enhanced activity for the degradation of rhodamine B and hydrogen evolution under visible light. *Diam. Relat. Mater.* **2022**, *125*, 109004. [CrossRef]
65. Atacan, K.; Güy, N.; Boutra, B.; Özacar, M. Enhancement of photoelectrochemical hydrogen production by using a novel ternary Ag_2CrO_4/GO/$MnFe_2O_4$ photocatalyst. *Int. J. Hydrogen Energy* **2020**, *45*, 17453–17467. [CrossRef]
66. Nivetha, R.; Chella, S.; Kollu, P.; Jeong, S.K.; Bhatnagar, A.; Andrews, N.G. Cobalt and nickel ferrites based graphene nanocomposites for electrochemical hydrogen evolution. *J. Magn. Magn. Mater.* **2018**, *448*, 165–171. [CrossRef]
67. Xu, X.; Azad, A.K.; Irvine, J.T.S. Photocatalytic H_2 generation from spinels $ZnFe_2O_4$, $ZnFeGaO_4$ and $ZnGa_2O_4$. *Catal. Today* **2013**, *199*, 22–26. [CrossRef]
68. Malik, A.Q.; Singh, H.; Kumar, A.; Aepuru, R.; Kumar, D.; Mir, T.u.G.; Ain, Q.u.; Bhat, A.A.; Mubayi, A. An Overview on Magnetic Separable Spinel as a Promising Materials for Photocatalysis and Waste Water Treatment. *ES Energy Environ.* **2022**, *19*, 744. [CrossRef]

69. Scheffe, J.R.; Allendorf, M.D.; Coker, E.N.; Jacobs, B.W.; McDaniel, A.H.; Weimer, A.W. Hydrogen Production via Chemical Looping Redox Cycles Using Atomic Layer Deposition-Synthesized Iron Oxide and Cobalt Ferrites. *Chem. Mater.* **2011**, *23*, 2030–2038. [CrossRef]
70. Peng, T.; Zhang, X.; Lv, H.; Zan, L. Preparation of $NiFe_2O_4$ nanoparticles and its visible-light-driven photoactivity for hydrogen production. *Catal. Commun.* **2012**, *28*, 116–119. [CrossRef]
71. Mangrulkar, P.A.; Joshi, M.M.; Tijare, S.N.; Polshettiwar, V.; Labhsetwar, N.K.; Rayalu, S.S. Nano cobalt oxides for photocatalytic hydrogen production. *Int. J. Hydrogen Energy* **2012**, *37*, 10462–10466. [CrossRef]
72. Dom, R.; Kumar, G.S.; Hebalkar, N.Y.; Joshi, S.V.; Borse, P.H. Eco-friendly ferrite nanocomposite photoelectrode for improved solar hydrogen generation. *RSC Adv.* **2013**, *3*, 15217–15224. [CrossRef]
73. Cheng, R.; Fan, X.; Wang, M.; Li, M.; Tian, J.; Zhang, L. Facile construction of $CuFe_2O_4$/g-C_3N_4 photocatalyst for enhanced visible-light hydrogen evolution. *RSC Adv.* **2016**, *6*, 18990–18995. [CrossRef]
74. Kim, H.S.; Kim, D.; Kwak, B.S.; Han, G.B.; Um, M.-H.; Kang, M. Synthesis of magnetically separable core@shell structured $NiFe_2O_4$@TiO_2 nanomaterial and its use for photocatalytic hydrogen production by methanol/water splitting. *Chem. Eng. J.* **2014**, *243*, 272–279. [CrossRef]
75. Police, A.K.R.; Basavaraju, S.; Valluri, D.K.; Muthukonda, V.S.; Machiraju, S.; Lee, J.S. $CaFe_2O_4$ sensitized hierarchical TiO_2 photo composite for hydrogen production under solar light irradiation. *Chem. Eng. J.* **2014**, *247*, 152–160. [CrossRef]
76. Hong, D.; Yamada, Y.; Sheehan, M.; Shikano, S.; Kuo, C.-H.; Tian, M.; Tsung, C.-K.; Fukuzumi, S. Mesoporous Nickel Ferrites with Spinel Structure Prepared by an Aerosol Spray Pyrolysis Method for Photocatalytic Hydrogen Evolution. *ACS Sustain. Chem. Eng.* **2014**, *2*, 2588–2594. [CrossRef]
77. Ortega López, Y.; Medina Vázquez, H.; Salinas Gutiérrez, J.; Guzmán Velderrain, V.; López Ortiz, A.; Collins Martínez, V. Synthesis Method Effect of $CoFe_2O_4$ on Its Photocatalytic Properties for H_2 Production from Water and Visible Light. *J. Nanomater.* **2015**, *2015*, 76. [CrossRef]
78. Dom, R.; Chary, A.S.; Subasri, R.; Hebalkar, N.Y.; Borse, P.H. Solar hydrogen generation from spinel $ZnFe_2O_4$ photocatalyst: Effect of synthesis methods. *Int. J. Energy Res.* **2015**, *39*, 1378–1390. [CrossRef]
79. Boudjemaa, A.; Popescu, I.; Juzsakova, T.; Kebir, M.; Helaili, N.; Bachari, K.; Marcu, I.-C. M-substituted (M = Co, Ni and Cu) zinc ferrite photo-catalysts for hydrogen production by water photo-reduction. *Int. J. Hydrogen Energy* **2016**, *41*, 11108–11118. [CrossRef]
80. Liu, J.; Zhu, D.; Ling, T.; Vasileff, A.; Qiao, S.-Z. S-$NiFe_2O_4$ ultra-small nanoparticle built nanosheets for efficient water splitting in alkaline and neutral pH. *Nano Energy* **2017**, *40*, 264–273. [CrossRef]
81. Zhang, H.; Nengzi, L.-c.; Li, B.; Cheng, Q.; Gou, J.; Cheng, X. Successfully synthesis of $FeSe_2$/$CoFe_2O_4$ heterojunction with high performance for hydrogen evolution reaction. *Renew. Energy* **2020**, *155*, 717–724. [CrossRef]